



Synthesis, Characterization, Biological Activity of PEG Capped Silver Nanoparticles and Photocatalytic Degradation of Methylene Blue Dye using LC-MS Method

RESHMA^{1,2,*}, HUSSAIN SHAIK³, KONDA MANOHAR⁴, B. MUKESH⁴,
RAMANA REDDY BODDU⁴, SRAVANTHI ITTIKYALA⁴ and PUPPALA VEERA SOMAIAH¹

¹Department of Chemistry, University College of Science, Osmania University, Tarnaka, Hyderabad-500007, India

²Chemistry Division, Department of Humanities & Sciences, CVR College of Engineering, Hyderabad-501510, India

³Analytical and Structural Chemistry Department, CSIR-Indian Institute of Chemical Technology, Tarnaka, Hyderabad-500007, India

⁴Vignan Institute of Technology & Science, Deshmukhi (V), Pochampally (M), Yadadri-Bhuvanagiri District-508284, India

*Corresponding author: E-mail: reshma1947aug15@gmail.com

Received: 9 December 2022;

Accepted: 20 September 2023;

Published online: 31 October 2023;

AJC-21427

Silver nanoparticles (AgNPs) were prepared by co-precipitation method using a capping agent, PEG-4000 (polyethylene glycol). The synthesized AgNPs were characterized using UV-visible, FTIR, SEM, EDX and TEM techniques. The bandgap energy of synthesized nanoparticles was determined using UV-visible spectra and found to be 3.07 eV. The particle size of nanoparticles calculated from the TEM and XRD pattern was in the range of 10-23 nm. The degradation efficiency of PEG capped AgNPs towards methylene blue (MB) dye under solar radiation was 63.78%. The photocatalytic degradation of MB dye follows the pseudo-first-order kinetics with an apparent rate constant of $1.1 \times 10^{-2} \text{ min}^{-1}$. The degradation products of MB dye during the photocatalytic process were identified using liquid chromatography-mass spectrometry (LC-ESI-TOF-MS). The antibacterial activity of synthesized PEG capped AgNPs using a disc diffusion method against four different Gram-positive and Gram-negative bacterial strains. The results showed that the synthesized nanoparticles could exhibit antibacterial activity. The anticancer activity of synthesized PEG capped AgNPs was tested against cancer cell lines such as A549 and HepG2. The results revealed that the synthesized PEG capped AgNPs have also shown an excellent anticancer activity with increasing their concentration. The antidiabetic activity of PEG capped AgNPs was studied against the α -glucosidase enzyme. The results confirmed that the synthesized AgNPs were shown α -glucosidase inhibition to 45.08%. The ABTS and DPPH radical scavenging activities were used to assay the antioxidant activity of synthesized PEG capped AgNPs.

Keywords: Silver nanoparticles, PEG-4000, Co-precipitation method, Biological activities, Photodegradation, Methylene blue dye.

INTRODUCTION

Silver nanoparticles (AgNPs) have gained tremendous recognition due to their potential uses in a variety of fields like oxidation catalysis, sensors, biomedicine, optics, electronics, fuel cells, photovoltaic cells, optical data storage systems, biological activity research, and so on [1-7]. The silver was widely recognized for antibacterial activity from ancient times. The silver nanoparticles are the most efficient antibacterial agents with a lower concentration than Ag^+ ions [8]. The biological inhibition activities of AgNPs rely upon a few morphological and physico-chemical such as size, shape and surface attributes that impact clearly in the accomplishment of these substances as antimicrobial agents. Enhanced antibacterial activity of the

AgNPs has appeared for the smallest particles inside the nanometer size range that seems to improve the permeability of silver particles in microbial cells, encouraging cell death. Moreover, the nearness of specific capping agents likewise improves their biocidal viability [9].

The capping agents (PEG-4000) are beneficial and play a crucial role in the synthesis of nanoparticles. They prevent self-agglomeration in the synthesis of nanoparticles and control their average size continuation. Coating polymers like polyethylene glycols are significant as they generate electrostatic repulsion between nanoparticles by steric effect and cause the size and structural stability [10]. The nanoparticle surface and polymeric chains are bonded with covalent and these interactions help increasing nanoparticle stability [11]. Several

chemical and physical methods are reported for the synthesis of silver nanoparticles [12,13]. Still, the most straightforward method is the co-precipitation, which involves chemically reducing metal salts to produce metal nanoparticles [14]. In view of this, we synthesized AgNPs by a simple co-precipitation method using PEG-4000 (polyethylene glycol) as a capping and stabilizing agent. The synthesized AgNPs were characterized by employing various physico-chemical techniques such as UV-visible, FTIR, XRD, SEM, EDS and TEM techniques. The synthesized nanoparticles were used in the photocatalytic degradation using methylene blue (MB) dye in the presence of solar irradiation. The degradation products were identified using liquid chromatography-mass spectrometry (LC-ESI-TOF-MS). The biological properties of synthesized nanoparticles were evaluated using the antibacterial, anticancer, antidiabetic and antioxidant activity studies.

EXPERIMENTAL

Analytical grade chemicals including silver nitrate, sodium hydroxide and polyethylene glycol (PEG-4000) were purchased from Merck, India. was purchased from Merck Specialties Ltd., India. Methylene blue dye was procured from Loba Chemie Pvt. Ltd., India, whereas the chemicals used for antibacterial activity were of Himedia grade, Mumbai, India. The bacterial test strains were procured from IMTECH, Chandigarh, India. The DPPH (2,2-diphenyl-1-picrylhydrazyl), ABTS [(2,2'-azino-di-(3-ethylbenthiazoline sulfonic acid)], *p*-nitrophenyl α -D-glucopyranoside and other chemicals were procured from Indian manufacturers.

Synthesis of AgNPs using PEG-400: Aqueous silver nitrate (0.2 M) solution was prepared in a clean, round bottom flask and then completely covered with aluminum foil to prevent the photoreduction. The 1% of PEG-400 was added to an aqueous AgNO₃ solution and heated to 80 °C with constant stirring. After few minutes, base solution (0.1 M NaOH) was added to a heated reaction mixture till pH reaches between 9 to 10 using NaOH solution. The reaction mixture was turned from dark brown to black colour, which confirmed the formation of silver nanoparticles. The precipitate was centrifuged, washed with deionized water and finally dried in a hot-air oven for 24 h. The obtained PEG-400 capped AgNPs were further used to confirm their structural, size and optical properties using physico-chemical methods and photocatalytic degradation and biological studies.

Characterization: The UV-Visible absorption analysis of synthesized AgNPs was recorded in the range of 200-800 nm by using Shimadzu UV-3600. The FTIR spectral analysis was recorded using a spectrophotometer (make: Bruker Optics, Germany) within the range of 4000-400 cm⁻¹. Powder X-ray diffraction (XRD) analysis of synthesized AgNPs with different capping agents was performed using X'pert Pro diffractometer (Panalytical B.V., The Netherlands) and samples analyses were performed within the range of $2\theta = 10^\circ$ - 80° , operating at 40 kV and a current of 30 mA with a nickel-filtered, CuK α ($\lambda = 1.5405 \text{ \AA}$) radiation. The surface morphology and elemental composition of synthesized AgNPs were evaluated using SEM and EDX, respectively using Zeiss evo18 SEM instrument,

whereas the TEM analysis was carried out using a transmission electron microscope (TEM, TecchnaiG2) instrument.

Antibacterial activity: The antibacterial activity of the synthesized AgNPs was evaluated using a suitable diffusion method and disc diffusion method [15-17] against different Gram-positive and Gram-negative pathogenic bacterial strains. The bacterial grade agars (2.5 g), NaCl (1 g), tryptophan (1 g) and yeast extract (0.5 g) were dissolved in double distilled water (100 mL) to prepare Luria-Bertani agar media. This media was sterilized using autoclaving at 120 °C temperature and a pressure of 15 psi for 60 min and followed by transferred it into sterilized Petri dish in laminar airflow. The different bacterial strains with an equal volume (100 μ L) were spread separately over the surface of the media. Finally, the petri plates were incubated at 37 °C for 24 h and then the inhibition zone was measured.

Anticancer activity

Cell viability assay (MTT assay): The cell viability (MTT assay) was used to assess the anticancer activity of synthesized AgNPs in 96-well plates [18-20]. The 5000 cells were seeded in each well and kept them for overnight incubation at 37 °C. The various concentrations of synthesized AgNPs were prepared and treated to cells on the next day. The experiment was carried out in triplicate wells. The experiment was terminated by removing media and then adds MTT containing media. The whole media was removed after 3 h of incubation in MTT containing media. The reduction of MTT formed the formazan crystals. Each well was dissolved by the addition of 50 μ L of DMSO:methanol (1:1 ratio) mixture.

$$\text{Cell viability (\%)} = \frac{\text{Mean absorbance of sample} - \text{Blank}}{\text{Mean absorbance of untreated} - \text{Blank}} \times 100$$

Cells and cell culture conditions: The anticancer activity of synthesized Ag NPs was evaluated against A549 and HepG2. These cells were procured from NCCS, Pune, India. The cells were inoculated and grown in Dulbecco Modified Eagle's Medium (DMEM) supplemented with 10% fetal bovine serum (FBS) and 1% antibiotics (penicillin and streptomycin), then incubated for 24 h in a humidified 5% CO₂ incubator (Thermo-Scientific) at 37 °C. The cells were incubated overnight under physiological conditions prior to their utilization in the cell viability experiment.

Preparation of samples: The 1XPBS (phosphate buffer saline) was used for making stocks of synthesized AgNPs. The working concentrations were prepared by diluting complete medium containing 10% FBS and antibiotics with 1X PBS stocks.

Antidiabetic activity: The antidiabetic activity of the synthesized AgNPs was evaluated using α -glucosidase enzyme. A solution of normal saline (100:1, w/v) was used for the dissolution of acetone power followed by sonication. After centrifuging the solvent at 4 °C and 4000 rpm for 0.5 h, the top layer of solvent was collected. This enzyme was originally thought to be a simple form of intestinal α -glucosidase. Phosphate buffer saline (pH 6.8) was utilized for the enzyme pre-incubation for 5 min. The resultant was reacted with substrate *p*-nitrophenyl- α -D-glucopyranoside, prepared in the same buffer, phosphate

buffer saline (pH 6.8) for 6 min. The *p*-nitrophenol was released due to the α -glucosidase enzyme action and it was measured spectrophotometrically at 405 nm. Acarbose was used a working standard and the percentage of inhibition α -glucosidase enzyme (λ_{max} : 405 nm) was calculated as follows:

$$\text{Inhibition (\%)} = \frac{A_{\text{control}} - A_{\text{sample}}}{A_{\text{control}}} \times 100$$

Antioxidant activity: The antioxidant activity of synthesized PEG-400 capped AgNPs was evaluated using ABTS and DPPH radicals.

ABTS radical scavenging activity: The ABTS radical scavenging activity of synthesized PEG-400 capped AgNPs was performed as per reported method [20]. Briefly, 100 mL ABTS (0.5 mM) stock solution was prepared by using potassium persulfate (6.89 Mm phosphate buffer solution (PBS), pH 8.0). The resultant solution mixture was stored in dark for overnight (~ 16 h). The synthesized nanoparticles (10 μ L of 2 mg/mL) and 190 μ L of ABTS solution were used for this study. These two solutions were added in a 96-well microplate. This experiment was carried out using the multimode microplate reader (BioTek^{synergy4}). After 15 min of incubation in dark, the absorbance analysis of decolourized ABTS radical was carried out at 734 nm. The ascorbic acid was used as a standard radical scavenger.

$$\text{Radical scavenging (\%)} = \frac{A_{\text{control}} - A_{\text{sample}}}{A_{\text{control}}} \times 100$$

DPPH radical scavenging activity: The synthesized AgNPs nanoparticles (25 μ L of 2 mg/mL), tris-HCl buffer (0.1 M, pH 7.4) and 125 μ L DPPH solution (0.5 Mm methanol) were taken in a 96-well microplate. The resultant solution was incubated in dark for 30 min and then the multimode microplate reader (BioTek^{synergy4}) was used to measure the absorbance of DPPH radical. The absorbance analysis of decolourized DPPH was carried out using spectrophotometrically at 517 nm after the incubation for 20 min. The intensity of DPPH was decreased in the presence of synthesized nanoparticles. The results revealed that the DPPH was decolourized during the reaction. Ascorbic acid was used as a standard radical scavenger. The following equation calculated the percentage of inhibition of DPPH radicals scavenging (λ_{max} : 517 nm).

$$\text{Radical scavenging (\%)} = \frac{A_{\text{control}} - A_{\text{sample}}}{A_{\text{control}}} \times 100$$

Photocatalytic degradation of methylene blue (MB) dye:

The photocatalytic activity of synthesized AgNPs was evaluated using methylene blue (MB) dye. The degradation of MB dye was evaluated using the catalyst (AgNPs) under solar irradiation. The MB dye is an organic dye and uses in textile industries for colouring. In this experiment, 30 mg of synthesized AgNPs were dispersed in 30 mL of double-distilled water and sonicated for 5 min. The resultant sample solution was added to 30 mL of MB dye solution (2×10^{-5} M) in a conical flask. The resultant mixed solution was stirred for a few minutes and sonicated for 0.5 h in the darkroom. Then the experiment was carried out on a maximum sunny day between 11 am to 4

pm (at 33–36 °C). The mixed reaction solution was kept under solar irradiation with constant stirring. At regular intervals, a 2 mL aliquot of the reaction mixture was taken out, filtered, and the solid phase was discarded. The resultant filtrate was tested by recording the absorbance at 664 nm by using a UV-visible spectrophotometer. The absorbance of MB dye was decreased at 664 nm (λ_{max}) with increasing the reaction time. The results revealed that MB dye was decolourized and degraded into new intermediate products [21–23]. The percentage of MB dye molecule degradation was calculated using the following equation:

$$\text{Degradation (\%)} = \frac{A_0 - A_t}{A_0} \times 100$$

where A_0 = initial absorption of MB dye, A_t = absorbance of MB dye at the time, t .

Photocatalytic degradation kinetic study: The kinetic study of photocatalytic degradation of MB dye was evaluated by using synthesized AgNPs under solarlight irradiation. The Langmuir-Hinshelwood kinetic model can explain the photocatalytic degradation of organic dyes using heterogeneous photocatalyst [24]. The following equation can apply for the photocatalytic reaction of dyes:

$$\text{Rate (r)} = \frac{dC}{dt} = \frac{kKC}{1 + KC}$$

However, for the low concentration of dyes, $KC \ll 1$ and then followed by integrating concerning time t , the resultant equation is $\ln(C_0/C_t) = k_{\text{app}} t$. It is a pseudo-first-order kinetic model equation.

Then, the equation is modified as:

$$\ln\left(\frac{A_0}{A_t}\right) = K_{\text{app}} t$$

where dC/dt = rate of dye degradation (mg/L min⁻¹), k = the reaction rate constant (min⁻¹), K = the absorption coefficient of the dye on to the photocatalyst, K_{app} (min⁻¹) is the apparent rate constant.

Liquid chromatography-mass spectrometry (LC-ESI-TOF-MS) analysis: In this experiment, it was used to identify the intermediate products/degradation products of MB dye in the presence of synthesized AgNPs during the photocatalytic reaction. The degradation products were determined using electrospray ionization in positive mode (MS-ESI⁺) and the time of flight analyzer (TOF) was used for this study [25]. The identification of intermediates products of MB dye was carried out using equity H class UPLC system (Waters, Milford, MA, USA) is coupled with Xevo G2-XS QTOF mass spectrometer (Waters, Manchester, UK). LC has conditioned with autosampler using an Acquity BEH C18 column (100 mm \times 2.1 mm i.d., 1.7 μ m particle size) (Waters, Milford, MA, USA). LC-MS gradient method conditions are given in Table-1. The LC was connected with a mass spectrometer, Xevo G2-XS QTOF (Waters, Manchester, U.K.). The mass instrument parameters are given in Table-2. The MassLynx v 4.1. software was used for the data acquisition. The stock solution of standard methylene blue dye (1 mg/mL) was prepared with doubled distilled

TABLE-1
LC-MS METHOD GRADIENT CONDITION DURING
THE PHOTOCATALYTIC DEGRADATION
OF METHYLENE BLUE DYE

Column	C18: 100 mm
Flow rate	0.2 mL/min
Run time	3 min
Buffers	1. H ₂ O with 0.1% FA 2. CAN with 0.1% FA
Source	ESI (Electrospray ionization)
Polarity	ESI-Positive mode
Column temperature	40 °C
Solubility of standard	Water
LC-MS gradient	Isocratic (A: 15%; B: 85%)

TABLE-2
MASS PARAMETERS DURING THE PHOTOCATALYTIC
DEGRADATION OF METHYLENE BLUE DYE

Capillary voltage	3.0 kv
Sample cone	30 V
Source temperature	120 °C
Desolvation temperature	350 °C
Cone gas flow rate	50 L/h
Desolvation gas (N ₂) flow rate	1000 L/h
Mass reference (lock spray)	Leucine-Enkephalin
Mass range	<i>m/z</i> 50 to 8000
Scan type	Ms full scan

water and further diluted it upto 1 µg/mL using the same solvent. The concentration, 1 µg/mL, was injected into LC-MS for studies and 5 mg/mL of synthesized nanoparticles were used for the evaluation of photodegradation studies.

RESULTS AND DISCUSSION

UV-visible studies: The UV-visible absorption spectra of synthesized PEG capped AgNPs are shown in Fig. 1. The AgNPs exhibit their absorption in the visible region [26,27]. The synthesized PEG capped AgNPs showed an absorbance in the UV-visible spectrum at 404 nm and the corresponding bandgap energy was 3.07 eV [28-30].

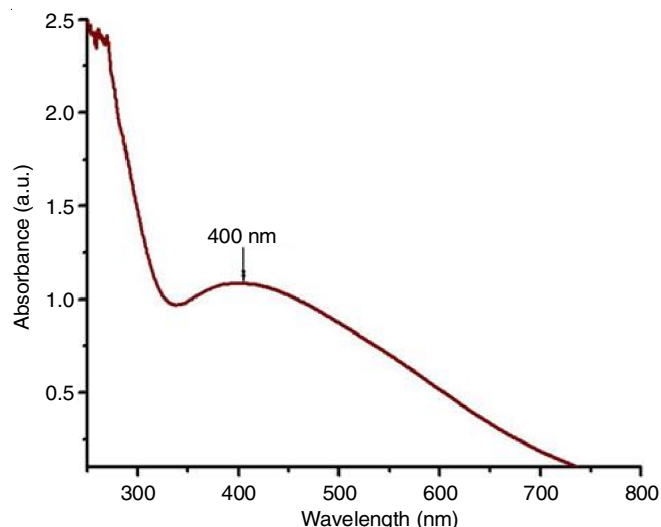


Fig. 1. UV-visible spectra of PEG capped AgNPs

FTIR studies: FTIR spectra of pure PEG and PEG capped AgNPs were performed in the range of 4000-400 cm⁻¹ and are shown in Fig. 2a-b, respectively. The results revealed the broad band appeared at 3390 cm⁻¹ was assigned to the O-H stretching vibrations of a hydroxyl group. The strong band at 1427 cm⁻¹ was due to C-H scissors and bending vibrations of alkanes. The low band at 1133 cm⁻¹ was attributed to stretching vibrations C-O of alcohol or C-O-C of ethers from PEG that indicating the formation of a coordinate bond between the oxygen atom of PEG and the Ag⁺ ions. The results revealed that the synthesized AgNPs were capped with polymer PEG [31-33].

XRD studies: Fig. 3 shows the XRD pattern of synthesized PEG capped AgNPs. The XRD pattern showed that the intensive and wide diffraction peaks at 2θ = 32.20°, 37.78°, 65.78° and 76.98° corresponds to (111), (200), (220) and (311) sets of lattice planes of AgNPs, respectively. The XRD pattern of PEG capped AgNPs showed that the synthesized nanoparticles are in the face-centric cubic (FCC) structure. These results were matched with JCPDS file no. 04-0783 [34,35]. The average

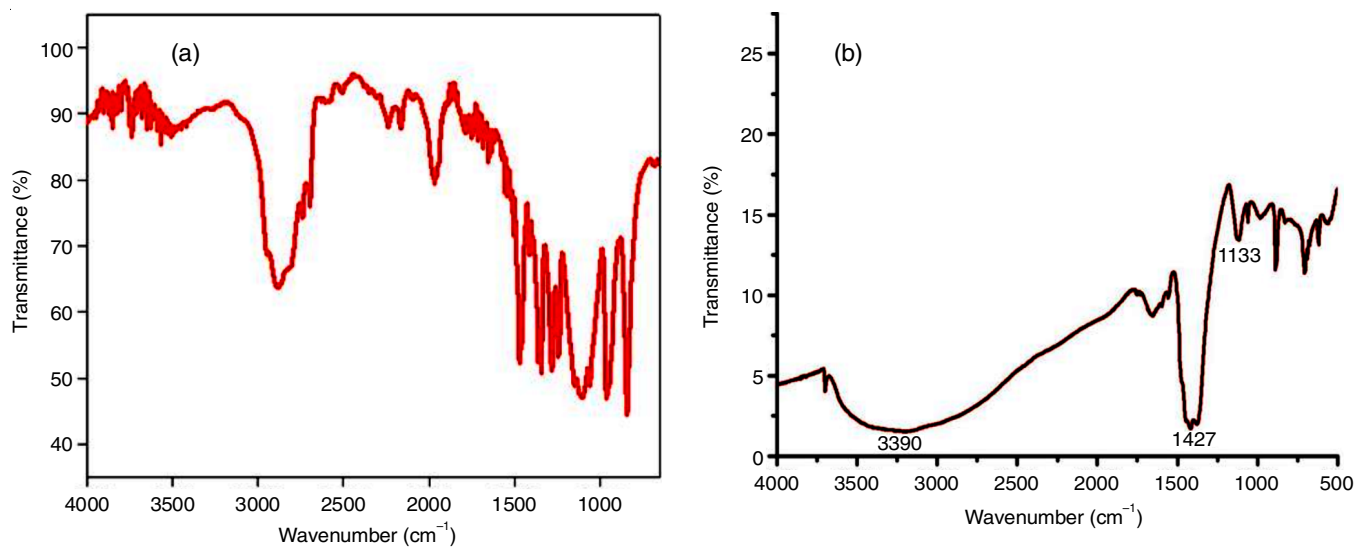


Fig. 2. FTIR spectra of (a) polyethyleneglycol (PEG) and (b) PEG capped AgNPs

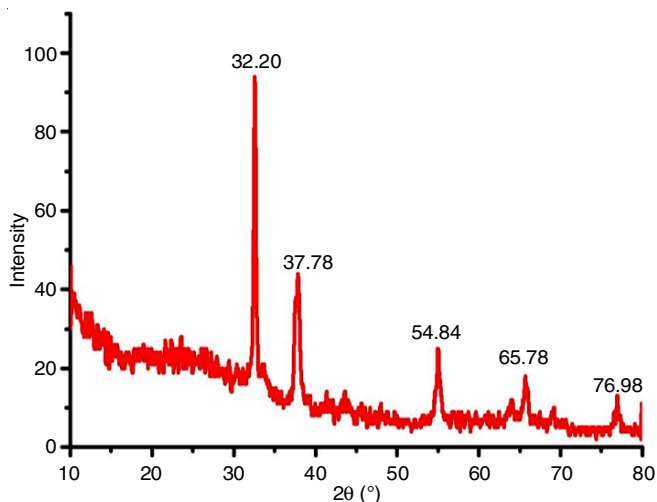


Fig. 3. XRD pattern of PEG capped AgNPs

size of synthesized PEG capped AgNPs was determined using Debye-Scherrer's formula.

$$D = \frac{K\lambda}{\beta \cos \theta} \tag{1}$$

From eqn. 1, the average size of synthesized PEG capped AgNPs were found in the range of 12-23 nm.

Morphological studies: The SEM images (Fig. 4) illustrated that the synthesized PEG capped AgNPs have a smooth surface with irregularly shape morphologies. The synthesized AgNPs showed a peak at ~3 KeV in the EDX spectra, indicating the synthesized AgNPs were in crystalline nature. The EDX results indicated that the synthesized PEG capped AgNPs contains Ag element and other element, oxygen. The presence of oxygen indicates that the presence of PEG as a capping agent on the surface of AgNPs [36,37].

TEM and SAED images of PEG capped AgNPs are shown in Fig. 5a-d. The results illustrated that the synthesized PEG capped AgNPs are not perfectly spherical and the size of nanoparticles was found in the range of 10 to 20 nm. The SAED pattern of the PEG capped AgNPs shows the different diffraction planes of AgNPs. The results showed that the PEG capped AgNPs are not perfectly spherical and uniformly distributed [38].

Antibacterial activity: The antibacterial activity was carried out by using a disc diffusion method against different bacterial strains. The Gram-negative strains of *Klebsiella pneumonia*, *Pseudomonas putida* and Gram-positive strains of *Bacillus subtilis*, *Staphylococcus aureus* bacteria were used to evaluate the antibacterial activity of synthesized PEG capped AgNPs. The standard ampicillin was used as a control. Each sample (50 μL) such as ampicillin, PEG capped AgNPs, NaOH solution and PEG was used and labeled as 1, 2, 3 and 4, respectively. The results of the zone of inhibition in mm for different bacteria are observed. The zone of inhibition for synthesized PEG capped Ag nanoparticles was found to be 7, 8, 7 and 9 mm for *Bacillus subtilis*, *Klebsiella pneumonia*, *Pseudomonas putida* and *Staphylococcus aureus*, respectively. The control group, treated with ampicillin, had measurements of 16 mm, 9 mm, 12 mm and 14 mm. The findings of this study indicate that AgNPs coated with PEG exhibit significant antibacterial properties [39-41].

Anticancer activity studies: The anticancer activity of synthesized PEG capped AgNPs was also tested against cancer cell lines such as A549 and HepG2. The anticancer results of synthesized nanoparticles are shown in Figs. 6 and 7. The different concentrations of synthesized PEG capped AgNPs were used for this activity. The results revealed that the synthesized PEG capped AgNPs have shown an excellent anticancer activity with increasing their concentration [42-44].

Antidiabetic activity studies

α-Glucosidase enzyme inhibition activity: The antidiabetic activity of PEG capped AgNPs was studied against the α-glucosidase enzyme [45,46]. The results confirmed that the synthesized AgNPs were shown an excellent inhibition against α-glucosidase (Table-3).

TABLE-3
PEG CAPPED AgNPs WERE SHOWN ANTIOXIDANT ACTIVITY USING ABTS AND DPPH SCAVENGING FREE RADICALS

	% Inhibition (200 μg/mL)		
	ABTS	DPPH	α-Glucosidase
AgNPs	64.82 ± 0.61	44.36 ± 0.65	45.08 ± 0.70
Ascorbic acid	99.3 ± 0.14	66.1 ± 1.75	–
Acarbose	–	–	62.96 ± 0.54

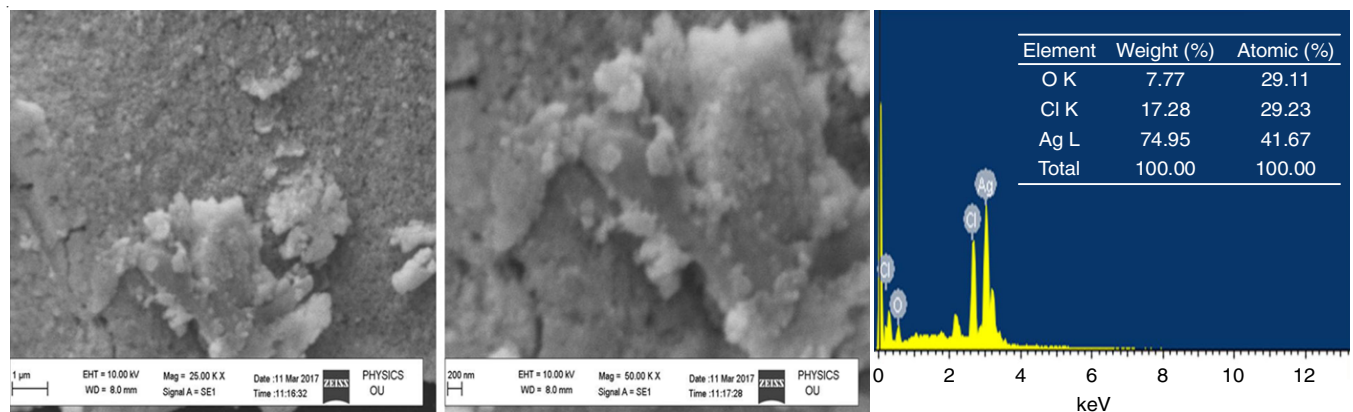


Fig. 4. SEM images and EDX spectra of PEG capped AgNPs

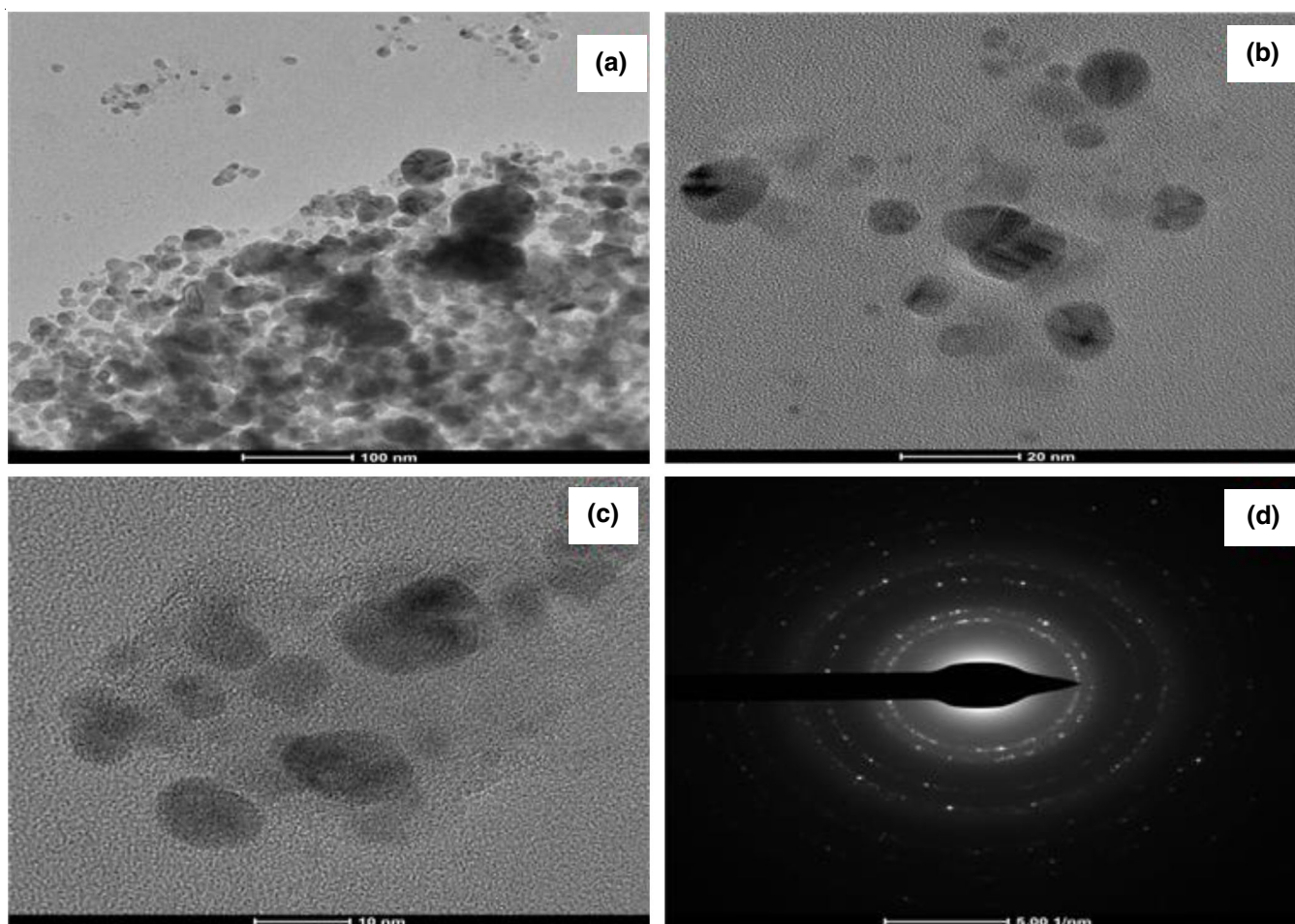


Fig. 5. (a-c) TEM images of PEG capped AgNPs (d) SAED image of PEG capped AgNPs

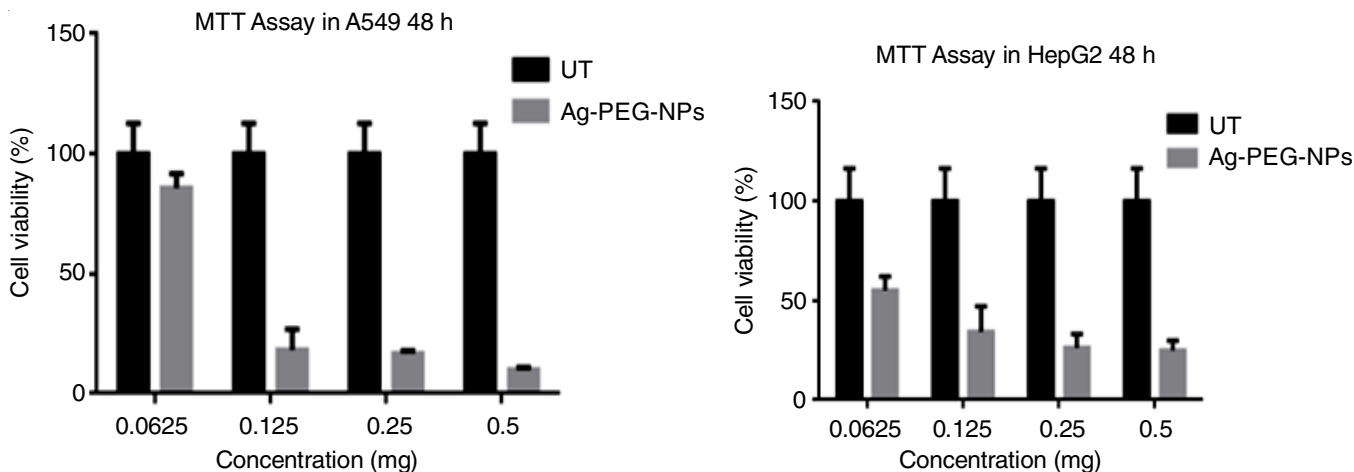


Fig. 6. Cell viability studies against cancer cell lines (A549 and HepG2) using MTT assay for 48 h with 0.0625, 0.125, 0.25 and 0.5 mg of synthesized PEG capped AgNPs

Antioxidant activity studies

ABTS and DPPH radical scavenging activity: The ABTS and DPPH radical scavenging activities were used to assay the antioxidant activity of PEG capped AgNPs. The hydrophilic antioxidant and lipophilic antioxidant nature of materials can be identified using ABTS radical. The other test model, DPPH, contains organic nitrogen centered radical and it is applied to

assess reducing the power of an antioxidant even with low redox potential [47,48]. The synthesized PEG capped AgNPs were showed antioxidant activity in the analysis. The results are shown in Table-3 and the values were represented as mean \pm standard deviation (N = 3).

Photocatalytic degradation of methylene blue dye: The photocatalytic degradation study of PEG capped AgNPs was

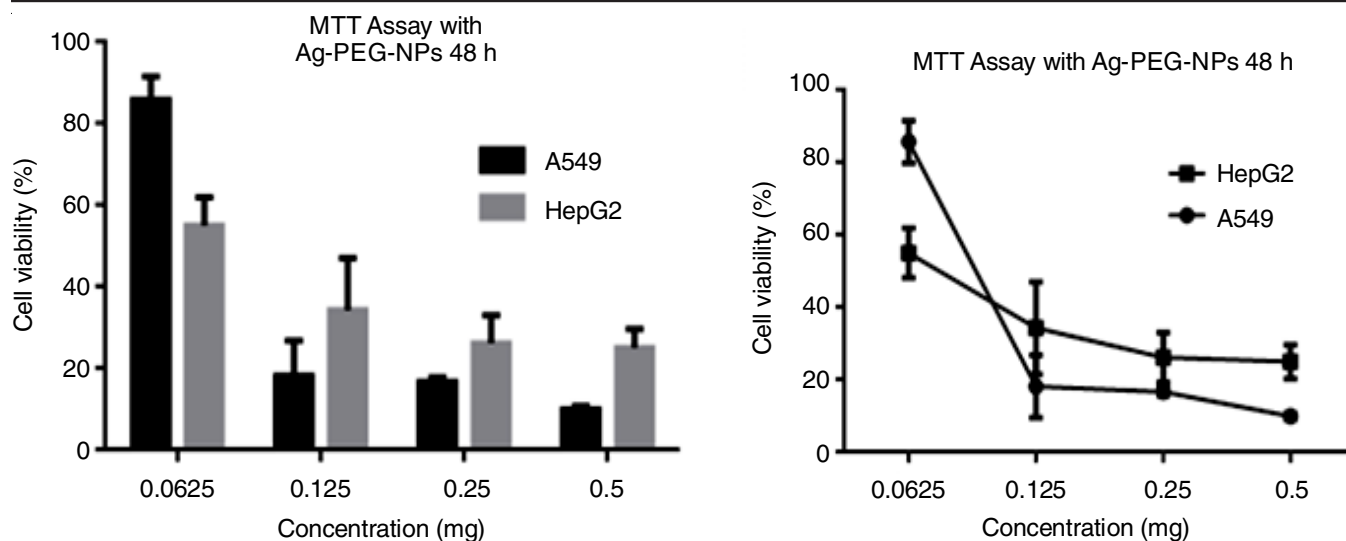


Fig. 7. Cell viability comparison between A549 and HepG2 cancer cells using MTT assay

evaluated using methylene blue dye under solar irradiation. The photocatalytic degradation reaction of MB dye was not effective without the addition of produced PEG capped AgNPs. The results of the study indicate that the addition of a catalyst or nanoparticles is essential for the decomposition of MB dye. An adsorption-desorption equilibrium was reached when PEG capped AgNPs was added to the MB dye solution. The UV-visible analysis of the degradation of MB dye using PEG capped AgNPs under solar irradiations is shown in Fig. 8. The absorbance of MB dye was gradually decreased during the photocatalytic reaction [49,50].

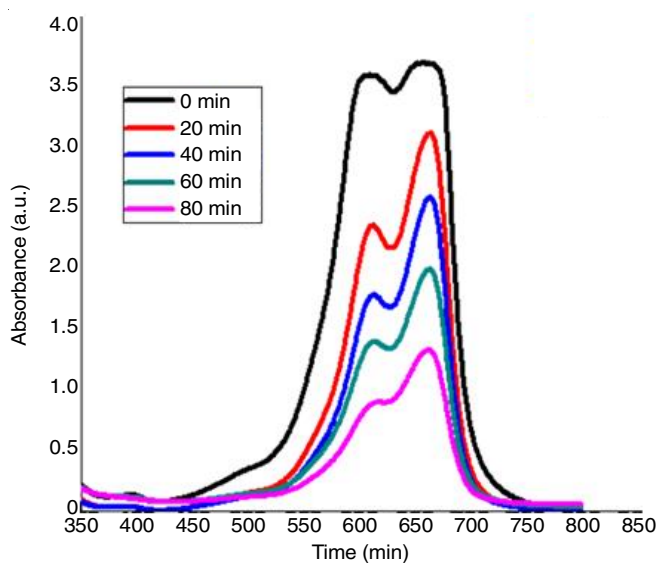


Fig. 8. UV-visible spectra of the photocatalytic degradation of methylene blue dye under solar irradiation in the presence of PEG capped Ag NPs

Percentage of degradation of MB dye: The percentage of degradation of MB dye using synthesized PEG capped AgNPs under solar irradiations was also studied in similar experimental conditions. The calculated degradation percentages of MB dye during the reaction are summarized in Table-4.

Time (min)	Degradation (%)
0	0
20	16.75
40	31.08
60	47.83
80	63.78

Photodegradation kinetics studies: During the process of the photocatalytic reactions, the Langmuir-Hinshelwood (L-H) equations are able to accurately represent the reactivity outcomes as well as the reaction rate of dye degradation [21]. The photocatalytic degradation of MB dye follows pseudo-first-order kinetics. The rate of the reaction was determined by plotting $\ln(A_0/A_t)$ versus the irradiation time of degradation of MB dye (Table-5).

Time (min)	A_0/A_t	$\ln(A_0/A_t)$
0	0	0
20	1.2	0.18
40	1.45	0.37
60	1.91	0.64
80	2.76	1.01

The rate constant (k) and correlating factor (R^2) values of photodegradation of MB dye using synthesized nanoparticles under solar light irradiations were found to be 1.1×10^{-2} and 0.966, respectively, which states that the photocatalytic degradation of MB dye follows a pseudo-first-order reaction (Fig. 9).

Identification of the degradation products of methylene blue during the photocatalytic degradation using UPLC-ESI-TOF-MS: The intermediate products/degraded products of MB dye during the photocatalytic degradation reaction was identified using a sophisticated liquid chromatography and

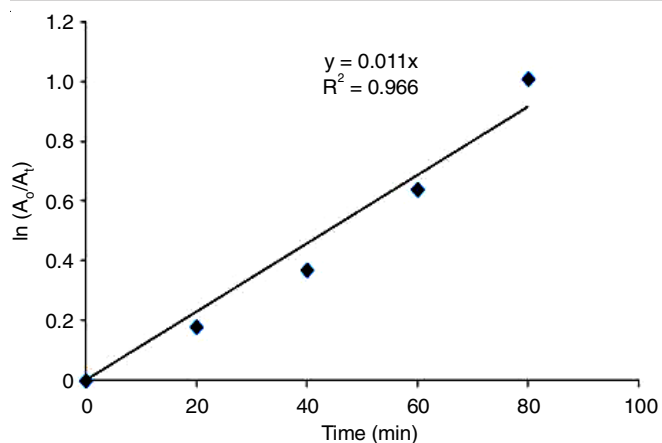


Fig. 9. The plots of $\ln(A_t/A_0)$ vs. time and the measured apparent rate constant K_{app} (min^{-1}) of the degradation of methylene blue dye using PEG capped AgNPs under solar irradiation

mass spectrometry (UPLC-ESI-TOF-MS) technique. The electrospray ionization (ESI) in positive mode was used in this experiment. Standard MB dye exhibits its characteristic absorption band at 664 nm (λ_{max}) in the UV-visible spectra. It gives a high intensive base peak at $m/z = 284$, corresponding to the M^+ molecular ion in the mass spectrometry (Figs. 10 and 11). In present study, the parent peak of MB dye after the addition of synthesized nanoparticles was observed with a decreased intensity (Fig. 11) and along with molecular ion, the various new peaks/products are formed. The results revealed that the MB dye was fragmented and formed new products. The photocatalytic process

mechanism stated that the decolourization of MB dye during the photocatalytic process due to adsorption as well as degradation in the presence of catalysts, PEG capped AgNPs. The MB dye possesses intense blue colour due to it contains chromophoric (N-S conjugated system on heteroaromatic cycle) and autochrome (lone pair electron on N atom in the heteroaromatic cycle) functional groups. These groups are essential to attain the high intense colour property of MB dye. In present investigation, the two possible mechanisms for the photocatalytic degradation of MB dye based on the decolourization mechanism and the type of degradation products are formed [51,52].

Chromophoric group degradation pathway: The first degradation pathway explains the chromophoric group degradation of methylene blue during the photocatalytic reaction in the presence of PEG capped AgNPs. The degradation products of methylene blue during chromophoric degradation were DP-6, DP-7, DP-8 and DP-9, which are shown in **Scheme-I**. The methylene blue dye gives its parent ion/molecular ion peak at m/z 284 in the mass spectrum and it further converts into various degradation products during chromophoric group degradation and resultant degradation products, including DP-6, DP-7, DP-8 and DP-9. The mechanism of chromophoric group degradation involves the electron reorganization in the methylene blue molecule, *i.e.* sulfhydryl ($C-S^+=C$) converts into sulfoxide ($C-S(=O)-C$). The degradation products of methylene blue dye *via* chromophoric degradation pathway during the photocatalytic reaction were identified using liquid chromatography-mass spectrometry (UPLC-ESI-TOF-MS).

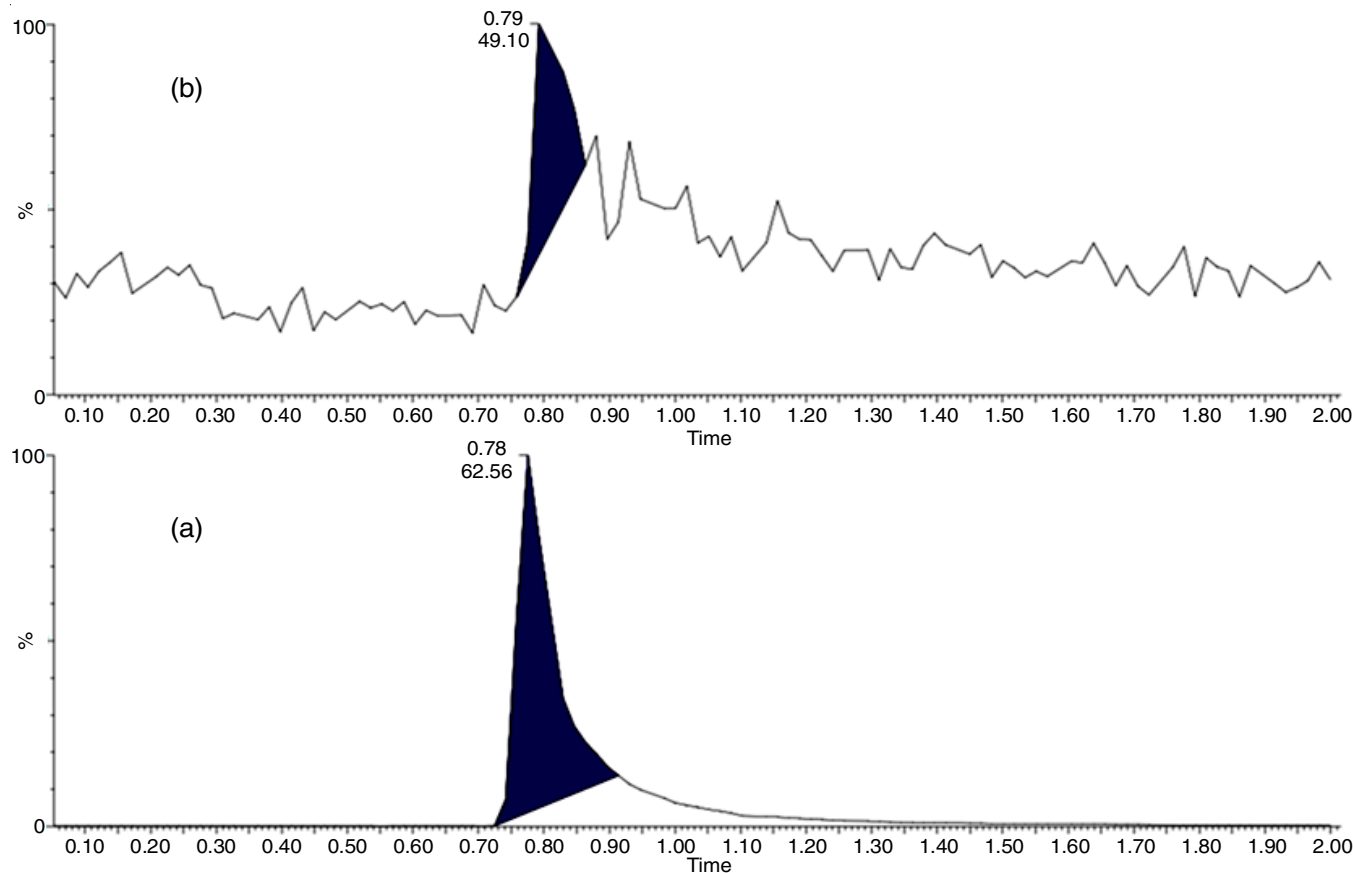


Fig. 10. TIC of methylene blue dye (a) and TIC of methylene blue after the addition of PEG capped AgNPs (b)

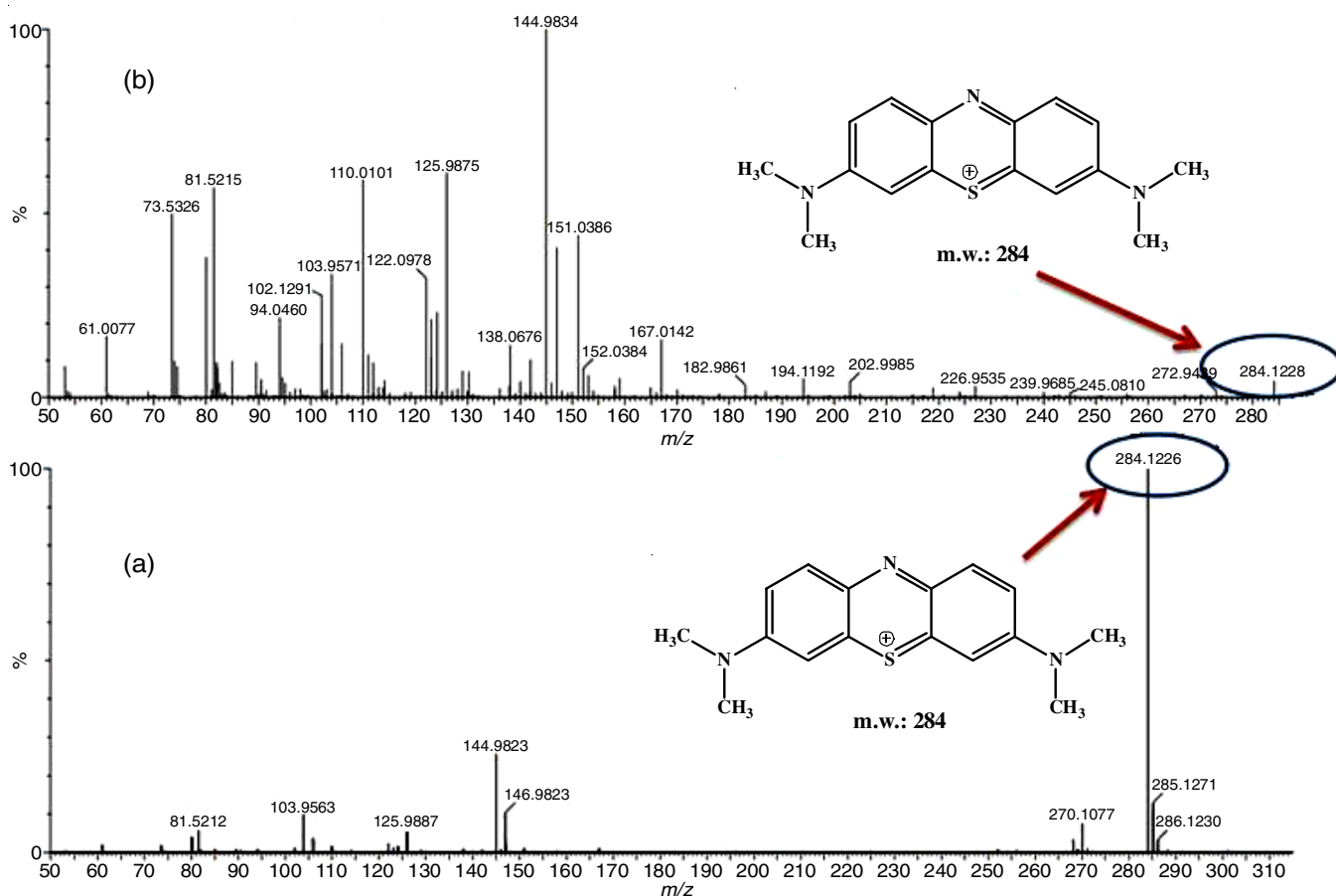
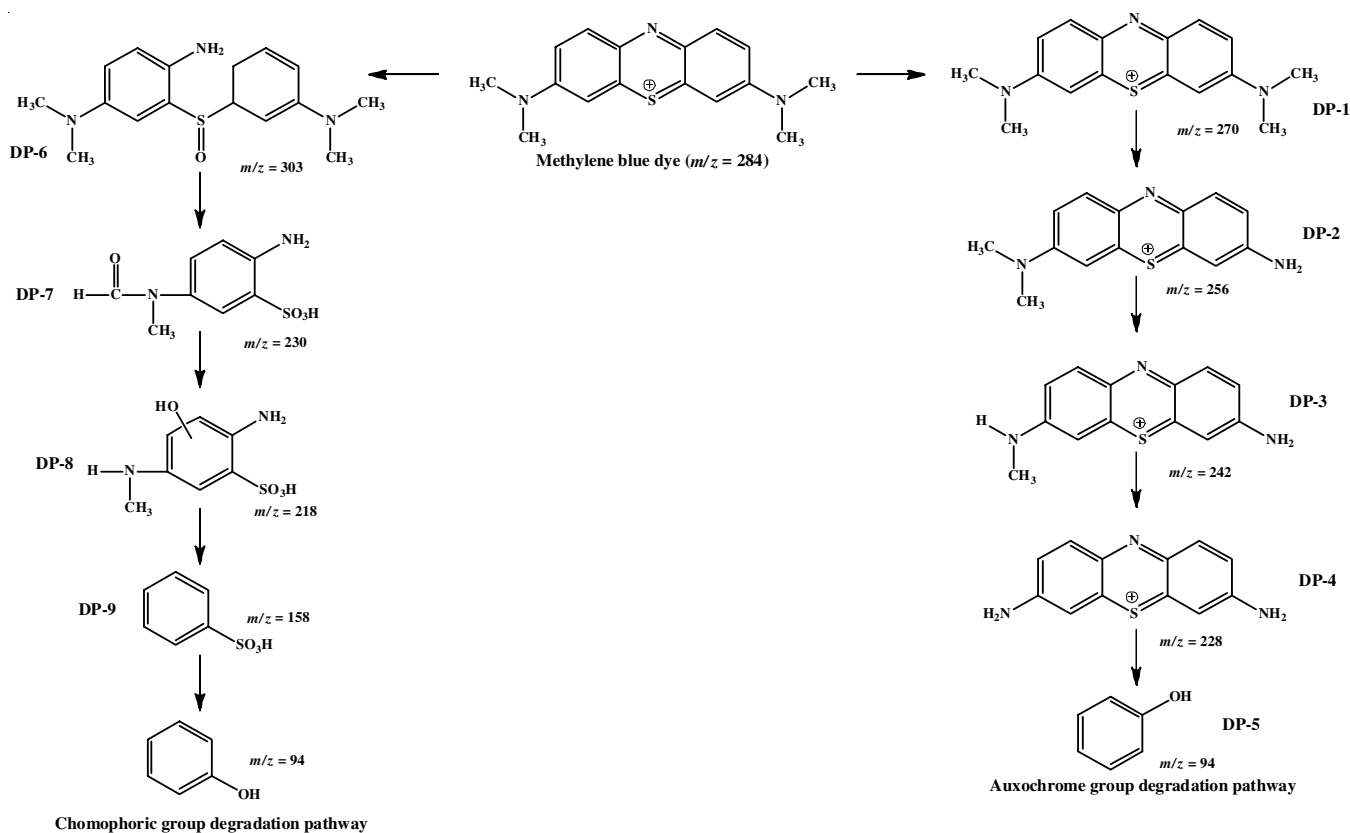


Fig. 11. Mass spectra of methylene blue dye (a) and the methylene blue dye after the addition of PEG capped AgNPs (b)



Scheme-I: Chromophoric and auxochrom degradation pathways of methylene blue dye

Auxochrome group degradation pathway: The second degradation pathway of methylene blue dye is an auxochrome group degradation. The degradation products of methylene blue dye *via* auxochrome group degradation were identified as DP-1, DP-2, DP-3, DP-4 and DP-5 using mass spectrometry and are shown in **Scheme-I**. The various degradation products of MB dye during the photocatalytic reaction were identified by using mass spectrometry are shown in Fig. 11.

The degradation products/intermediates products of MB dye during the photocatalytic reaction were identified using mass spectrometry (spectra not shown). These products were produced from two different degradation pathways of MB dye.

Conclusion

Silver nanoparticles (AgNPs) were synthesized by the co-precipitation method using polyethylene glycol (PEG-4000) as a capping and stabilizing agent. These nanoparticles were characterized by various techniques like UV-visible, FTIR, XRD, SEM, EDX and TEM. The particle size was found in the range of 10-23 nm by XRD and TEM analysis. The synthesized PEG capped AgNPs was applied in the photocatalytic degradation of methylene blue (MB) dye under solar irradiation. The degradation efficiency of PEG capped AgNPs towards MB dye in the presence under solar radiation was 63.78%. The Langmuir-Hinshelwood kinetic analyses revealed that the dye degradation followed the pseudo-first-order kinetics with apparent rate constant k_{app} value of $1.1 \times 10^{-2} \text{ min}^{-1}$. The degradation products of MB dye during the photocatalytic process were identified using liquid chromatography-mass spectrometry (LC-ESI-TOF-MS). The antibacterial activity of synthesized PEG capped AgNPs using a disc diffusion method against four different Gram-positive and Gram-negative bacterial strains. The results showed that the synthesized nanoparticles could exhibit antibacterial activity. The results also revealed that the synthesized PEG capped AgNPs have shown an excellent anticancer activity against the cancer cell lines such as A549 and HepG2 with increasing concentration. The α -glucosidase inhibition of 45.08% was also exhibited by the PEG capped AgNPs against the α -glucosidase enzyme. The antioxidant activity of synthesized nanoparticles was also examined using ABTS and DPPH radicals assay. The results showed that the synthesized PEG capped AgNPs could show antioxidant activity of 64.82% and 44.36% against ABTS and DPPH radical, respectively.

CONFLICT OF INTEREST

The authors declare that there is no conflict of interests regarding the publication of this article.

REFERENCES

1. F. Derikvand, F. Bigi, R. Maggi, C.G. Piscopo and G. Sartori, *J. Catal.*, **271**, 99 (2010); <https://doi.org/10.1016/j.jcat.2010.02.015>
2. W. Wang, Q. Zhao, J. Dong and J. Li, *Int. J. Hydrogen Energy*, **36**, 7374 (2011); <https://doi.org/10.1016/j.ijhydene.2011.03.096>
3. V.V. Petrov, T.N. Nazarova, A.N. Korolev and N.F. Kopilova, *Sens. Actuators B Chem.*, **133**, 291 (2008); <https://doi.org/10.1016/j.snb.2008.02.026>
4. E. Sanli, B.Z. Uysal and M.L. Aksu, *Int. J. Hydrogen Energy*, **33**, 2097 (2008); <https://doi.org/10.1016/j.ijhydene.2008.01.049>
5. Y. Ida, S. Watase, T. Shinagawa, M. Watanabe, M. Chigane, M. Inaba, A. Tasaka and M. Izaki, *Chem. Mater.*, **20**, 1254 (2008); <https://doi.org/10.1021/cm702865r>
6. W.X. Li, C. Stampfl and M. Scheffler, *Phys. Rev. B Condens. Matter*, **68**, 165412 (2003); <https://doi.org/10.1103/PhysRevB.68.165412>
7. G. Cabello-Carramolino and M.D. Petit-Dominguez, *Mikrochim. Acta*, **164**, 405 (2009); <https://doi.org/10.1007/s00604-008-0074-6>
8. C.N. Lok, C.M. Ho, R. Chen, Q.Y. He, W.Y. Yu, H. Sun, P.K.-H. Tam, J.-F. Chiu and C.-M. Che, *J. Proteome Res.*, **5**, 916 (2006); <https://doi.org/10.1021/pr0504079>
9. A. Panáček, L. Kvítek, R. Prucek, M. Kolář, R. Večeřová, N. Pizúrová, V.K. Sharma, T. Nevířná and R. Zbořil, *J. Phys. Chem. B*, **110**, 16248 (2006); <https://doi.org/10.1021/jp063826h>
10. C. Luo, Y. Zhang, X. Zeng, Y. Zeng and Y. Wang, *J. Colloid Interface Sci.*, **288**, 444 (2005); <https://doi.org/10.1016/j.jcis.2005.03.005>
11. T.H. Tran and V.T. Nguyen, *Int. Sch. Res. Notices*, **2014**, 856592 (2014); <https://doi.org/10.1155/2014/856592>
12. M. Zahoor, N. Nazir, M. Iftikhar, S. Naz, I. Zekker, J. Burlakovs, F. Uddin, A.W. Kamran, A. Kallistova, N. Pimenov and F.A. Khan, *Water*, **13**, 2216 (2021); <https://doi.org/10.3390/w13162216>
13. S. Irvani, H. Korbekandi, S.V. Mirmohammadi and B. Zolfaghari, *Res. Pharm. Sci.*, **9**, 385 (2014).
14. A. López-Serrano, R.M. Olivás, J.S. Landaluz and C. Cámara, *Anal. Methods*, **6**, 38 (2014); <https://doi.org/10.1039/C3AY40517F>
15. M. Balouiri, M. Sadiki and S.K. Ibsouda, *J. Pharm. Anal.*, **6**, 71 (2016); <https://doi.org/10.1016/j.jpha.2015.11.005>
16. L. Wang, C. Hu and L. Shao, *Int. J. Nanomedicine*, **12**, 1227 (2017); <https://doi.org/10.2147/IJN.S121956>
17. D. Ayodhya, M. Venkatesham, A.S. Kumari, G.B. Reddy, D. Ramakrishna and G. Veerabhadram, *J. Fluoresc.*, **25**, 1481 (2015); <https://doi.org/10.1007/s10895-015-1639-5>
18. M. Wypij, T. Jedrzejewski, J. Trzcinska-Wencel, M. Ostrowski, M. Rai and P. Golinska, *Front. Microbiol.*, **12**, 632505 (2021); <https://doi.org/10.3389/fmicb.2021.632505>
19. M.A. Siddiqui, M.P. Kashyap, V. Kumar, A.A. Al-Khedhairi, J. Musarrat and A.B. Pant, *Toxicol. in Vitro*, **24**, 1592 (2010); <https://doi.org/10.1016/j.tiv.2010.06.008>
20. A.S.R. Sailakshmi, A. Anand, K. Madhusudana, V.L. Nayak, A. Zehra, K.S. Babu and A.K. Tiwari, *Indian J. Natural Prod. Resour.*, **9**, 194 (2018).
21. D. Ayodhya, M. Venkatesham, A. Santoshi Kumari, G.B. Reddy, D. Ramakrishna and G. Veerabhadram, *J. Exp. Nanosci.*, **11**, 418 (2016); <https://doi.org/10.1080/17458080.2015.1070312>
22. M.N. Chong, B. Jin, C.W. Chow and C. Saint, *Water Res.*, **44**, 2997 (2010); <https://doi.org/10.1016/j.watres.2010.02.039>
23. N. Daneshvar, D. Salari and A.R. Khataee, *J. Photochem. Photobiol. Chem.*, **162**, 317 (2004); [https://doi.org/10.1016/S1010-6030\(03\)00378-2](https://doi.org/10.1016/S1010-6030(03)00378-2)
24. H. Al-Ekabi and N. Serpone, *J. Phys. Chem.*, **92**, 5726 (1988); <https://doi.org/10.1021/j100331a036>
25. J.J. Pitt, *Clin. Biochem. Rev.*, **30**, 19 (2009).
26. S. Chen, S. Webster, R. Czerw, J. Xu and D.L. Carroll, *J. Nanosci. Nanotechnol.*, **4**, 254 (2004); <https://doi.org/10.1166/jnn.2004.034>
27. S.S. Shankar, A. Ahmad and M. Sastry, *Biotechnol. Prog.*, **19**, 1627 (2003); <https://doi.org/10.1021/bp034070w>
28. X.F. Zhang, Z.G. Liu, W. Shen and S. Gurusathan, *Int. J. Mol. Sci.*, **17**, 1534 (2016); <https://doi.org/10.3390/ijms17091534>

29. M.M. Khan, S. Kumar, M. Ahamed, S.A. Alrokayan, M.S. Alsalhi, M. Alhoshan and A.S. Aldwayyan, *Appl. Surf. Sci.*, **257**, 10607 (2011); <https://doi.org/10.1016/j.apsusc.2011.07.058>
30. H. Kumar and R. Rani, *Int. J. Eng. Innov. Technol.*, **3**, 344 (2013).
31. M.B. Ahmad, M.Y. Tay, K. Shameli, M.Z. Hussein and J.J. Lim, *Int. J. Mol. Sci.*, **12**, 4872 (2011); <https://doi.org/10.3390/ijms12084872>
32. P. Raveendran, J. Fu and S.L. Wallen, *J. Am. Chem. Soc.*, **125**, 13940 (2003); <https://doi.org/10.1021/ja029267j>
33. K. Gupta, P.C. Jana and A.K. Meikap, *Synth. Met.*, **160**, 1566 (2010); <https://doi.org/10.1016/j.synthmet.2010.05.026>
34. M. Fu, Q. Li, D. Sun, Y. Lu, N. He, X. Deng, H. Wang and J. Huang, *Chin. J. Chem. Eng.*, **14**, 114 (2006); [https://doi.org/10.1016/S1004-9541\(06\)60046-3](https://doi.org/10.1016/S1004-9541(06)60046-3)
35. K. Shameli, M. Bin Ahmad, S.D. Jazayeri, S. Sedaghat, P. Shabanzadeh, H. Jahangirian, M. Mahdavi and Y. Abdollahi, *Int. J. Mol. Sci.*, **13**, 6639 (2012); <https://doi.org/10.3390/ijms13066639>
36. T.R. Dhakal, S.R. Mishra, Z. Glenn and B.K. Rai, *J. Nanosci. Nanotechnol.*, **12**, 6389 (2012); <https://doi.org/10.1166/jnn.2012.6561>
37. C. Díaz-Cruz, G. Alonso Nuñez, H. Espinoza-Gómez and L.Z. Flores-López, *Eur. Polym. J.*, **83**, 265 (2016); <https://doi.org/10.1016/j.eurpolymj.2016.08.025>
38. M. Roldán, N. Pellegrini and O. de Sanctis, *J. Nanoparticles*, **2013**, 524150 (2013); <https://doi.org/10.1155/2013/524150>
39. Z. Khan, M.A. Nisar, S.Z. Hussain, M.N. Arshad and A. Rehman, *Appl. Microbiol. Biotechnol.*, **99**, 10745 (2015); <https://doi.org/10.1007/s00253-015-6901-x>
40. M.R. Das, R.K. Sarma, R. Saikia, V.S. Kale, M.V. Shelke and P. Sengupta, *Colloids Surf. B Biointerfaces*, **83**, 16 (2011); <https://doi.org/10.1016/j.colsurfb.2010.10.033>
41. M.A. Shaker and M.I. Shaaban, *J. Taibah Univ. Med. Sci.*, **12**, 291 (2017); <https://doi.org/10.1016/j.jtumed.2017.02.008>
42. P. Gopinath, S.K. Gogoi, A. Chattopadhyay and S.S. Ghosh, *Nanotechnology*, **19**, 075104 (2008); <https://doi.org/10.1088/0957-4484/19/7/075104>
43. P.V. AshaRani, G. Low Kah Mun, M.P. Hande and S. Valiyaveetil, *ACS Nano*, **3**, 279 (2009); <https://doi.org/10.1021/nn800596w>
44. Z. Muhammad, A. Raza, S. Ghafoor, A. Naeem, S.S. Naz, S. Riaz, W. Ahmed and N.F. Rana, *Eur. J. Pharm. Sci.*, **91**, 251 (2016); <https://doi.org/10.1016/j.ejps.2016.04.029>
45. K. Rajaram, D.C. Aiswarya and P. Sureshkumar, *Mater. Lett.*, **138**, 251 (2015); <https://doi.org/10.1016/j.matlet.2014.10.017>
46. A. Hashim, I.R. Agool and K.J. Kadhim, *J. Bionanosci.*, **12**, 608 (2018); <https://doi.org/10.1166/jbns.2018.1580>
47. T. SivaKumar, T. Rathimeena, V. Thangapandian and T. Shankar, *J. Biosci. Bioeng.*, **1**, 22 (2015).
48. L. Wang, Y. Wu, J. Xie, S. Wu and Z. Wu, *Mater. Sci. Eng. C*, **86**, 1 (2018); <https://doi.org/10.1016/j.msec.2018.01.003>
49. E.M. Azzam, N.A. Fathy, S.M. El-Khouly and R.M. Sami, *J. Water Process Eng.*, **28**, 311 (2019); <https://doi.org/10.1016/j.jwpe.2019.02.016>
50. K. Roy, C.K. Sarkar and C.K. Ghosh, *Appl. Nanosci.*, **5**, 953 (2015); <https://doi.org/10.1007/s13204-014-0392-4>
51. C. Yang, W. Dong, G. Cui, Y. Zhao, X. Shi, X. Xia, B. Tang and W. Wang, *RSC Adv.*, **7**, 23699 (2017); <https://doi.org/10.1039/C7RA02423A>
52. S. Xia, L. Zhang, G. Pan, P. Qian and Z. Ni, *Phys. Chem. Chem. Phys.*, **17**, 5345 (2015); <https://doi.org/10.1039/C4CP03877K>